High-throughput in vivo screen of functional mRNA delivery identifies nanoparticles for endothelial cell gene editing

Cory D. Sago[a], Melissa P. Lokugamage[a], Kalina Paunovska[a], Daryll A. Vanover[a], Christopher M. Monaco[b], Nirav N. Shah[b], Marielena Gamboa Castro[a], Shannon E. Anderson[a], Tobi G. Rudoltz[a], Gwyneth N. Lando[a], Pooja Munnilal Tiwari[a], Jonathan L. Kirschman[a], Nick Willett[a,c,d,e], Young C. Jang[b], Philip J. Santangelo[a], Anton V. Bryksin[c], and James E. Dahlman[a,1]

[a]Wallace H. Coulter Department of Biomedical Engineering, Georgia Institute of Technology and Emory University School of Medicine, Atlanta, GA 30332; [b]School of Biological Sciences, Georgia Institute of Technology, Atlanta, GA 30332; [c]Parker H. Petit Institute for Bioengineering and Bioscience, Georgia Institute of Technology, Atlanta, GA 30332; [d]Department of Orthopaedics, Emory University, Atlanta, GA 30322; and [e]Atlanta Veterans Affairs Medical Center, Decatur, GA 30033

Edited by Michael B. A. Oldstone, The Scripps Research Institute, La Jolla, CA, and approved September 11, 2018 (received for review July 2, 2018)

Dysfunctional endothelium causes more disease than any other cell type. Systemically administered RNA delivery to nonliver tissues remains challenging, in large part because there is no high-throughput method to identify nanoparticles that deliver functional mRNA to cells in vivo. Here we report a system capable of simultaneously quantifying how >100 lipid nanoparticles (LNPs) deliver mRNA that is translated into functional protein. Using this system (named FIND), we measured how >250 LNPs delivered mRNA to multiple cell types in vivo and identified 7C2 and 7C3, two LNPs that efficiently deliver siRNA, single-guide RNA (sgRNA), and mRNA to endothelial cells. The 7C3 delivered Cas9 mRNA and sgRNA to splenic endothelial cells as efficiently as hepatocytes, distinguishing it from LNPs that deliver Cas9 mRNA and sgRNA to hepatocytes more than other cell types. These data demonstrate that FIND can identify nanoparticles with novel tropisms in vivo.

nanoparticle | CRISPR | RNAi | barcoded nanoparticle | mRNA

A lipid nanoparticle (LNP) siRNA therapy targeted to hepatocytes (1, 2) has been approved by the Food and Drug Administration (FDA). This advance is exciting, but its long-term implications are tempered by the fact that clinical LNP therapies have targeted hepatocytes (when administered systemically) (1, 3) and muscle (when administered locally) (4). In mice, nanoparticles have delivered Cas9 mRNA and ribonucleoproteins via systemic or local injection (5–12). Systemically administered Cas9 delivery to nonliver tissues remains a challenge. When LNPs are administered systemically, they display an affinity for the liver; this is thought to be driven by natural physiological advantages including slow blood flow (13, 14) and discontinuous vasculature in hepatic sinusoids (15). One additional reason most LNPs target the liver may be the process by which they are selected. LNPs are screened in vitro before a few LNPs are tested in vivo. In vitro LNP delivery can predict in vivo LNP delivery to hepatocytes (16), but in vitro nanoparticle can be a poor predictor of in vivo delivery to endothelial cells and macrophages (17). Moreover, LNP siRNA delivery is often tested in vivo using the FVII assay, which predicts hepatocyte delivery; this assay is enhanced by its ease, as well as the fact that validated, potent siRNA targeting FVII is available (18, 19). It is possible that LNPs target hepatocytes in part because established assays select for hepatocyte delivery.

We reasoned that measuring hundreds of distinct LNPs in vivo would provide the best chance of identifying nanoparticles that deliver mRNA to new cell types. Using DNA barcodes (17, 20–22), we previously quantified how >350 LNPs distributed in vivo. However, biodistribution is necessary, but not sufficient, for functional RNA delivery. Over 96% of RNA delivered into the endosome of a target cell can be degraded (23, 24), and cell-type-specific changes in endosomal escape are not understood (25). Thus, it is difficult to predict functional delivery using biodistribution. As a result, a high-throughput method to quantify functional, cytosolic delivery of mRNA in vivo could accelerate the discovery of clinically relevant LNPs.

An ideal system would (*i*) enable scientists to test many LNPs simultaneously, (*ii*) utilize commonly available animal models, (*iii*) rely on a robust signal, and (*iv*) measure functional RNA delivery to any combinations of cell types in vivo. Measuring delivery to "on-target" cells and "off-target" cells would enable iterative screens to improve LNP specificity. We designed a system named Fast Identification of Nanoparticle Delivery (FIND) that meets these criteria. FIND measures cytosolic mRNA delivery by >100 LNPs in vivo to any combination of cell types. We quantified how >250 LNPs functionally delivered mRNA to multiple cell types in vivo and identified two formulations that deliver RNA to endothelial beds. FIND is a system that facilitates high-throughput screens of functional mRNA delivery and may identify LNPs with novel tropisms.

Significance

Nanoparticle-mediated delivery of siRNA to hepatocytes has treated disease in humans. However, systemically delivering RNA drugs to nonliver tissues remains an important challenge. To increase the number of nanoparticles that could be studied in vivo, we designed a high-throughput method to measure how >100 nanoparticles delivered mRNA that was translated into functional protein in vivo. We quantified how >250 lipid nanoparticles (LNPs) delivered mRNA in vivo, identifying two LNPs that deliver mRNA to endothelial cells. One of the LNPs codelivered Cas9 mRNA and single-guide RNA in vivo, leading to endothelial cell gene editing. This approach can identify nanoparticles that target new cells.

Author contributions: C.D.S., M.P.L., N.W., Y.C.J., P.J.S., and J.E.D. designed research; C.D.S., M.P.L., K.P., D.A.V., C.M.M., N.N.S., M.G.C., S.E.A., T.G.R., G.N.L., P.M.T., J.L.K., A.V.B., and J.E.D. performed research; C.D.S., M.P.L., K.P., D.A.V., N.N.S., and J.E.D. contributed new reagents/analytic tools; C.D.S., M.P.L., C.M.M., P.M.T., N.W., Y.C.J., P.J.S., A.V.B., and J.E.D. analyzed data; and C.D.S., M.P.L., and J.E.D. wrote the paper.

Conflict of interest statement: C.D.S., M.P.L., and J.E.D. have filed intellectual property related to this publication.

This article is a PNAS Direct Submission.

[1]To whom correspondence should be addressed. Email: james.dahlman@bme.gatech.edu.

This article contains supporting information online at www.pnas.org/lookup/suppl/doi:10.1073/pnas.1811276115/-/DCSupplemental.

Published online October 1, 2018.

Results

FIND combined rationally designed DNA barcodes and the Cre-Lox system to generate a multiplexed readout of functional mRNA delivery. FIND is distinct from previous barcoding systems we developed, which measure biodistribution (Fig. 1*A*). Using high-throughput microfluidics (26), we coformulated LNPs with Cre mRNA and a unique DNA barcode. LNP-1, with chemical structure 1, carried DNA barcode 1 and Cre mRNA; LNP-N, with chemical structure N, carried DNA barcode N and Cre mRNA (Fig. 1 *A*–*C*). We characterized the size and stability of each LNP using dynamic light scattering (DLS) and discarded LNPs that did not meet two criteria: (*i*) diameters between 20 and 200 nm and (*ii*) an autocorrelation curve with one inflection point (*SI Appendix*, Fig. S1*A*). LNPs that met these criteria were pooled together and administered to Lox-Stop-Lox-tdTomato (Ai14) mice (27). Ai14 cells fluoresce if Cre mRNA is translated into Cre protein, which then translocates to the nucleus and edits target DNA. We isolated tdTomato$^+$ cells with

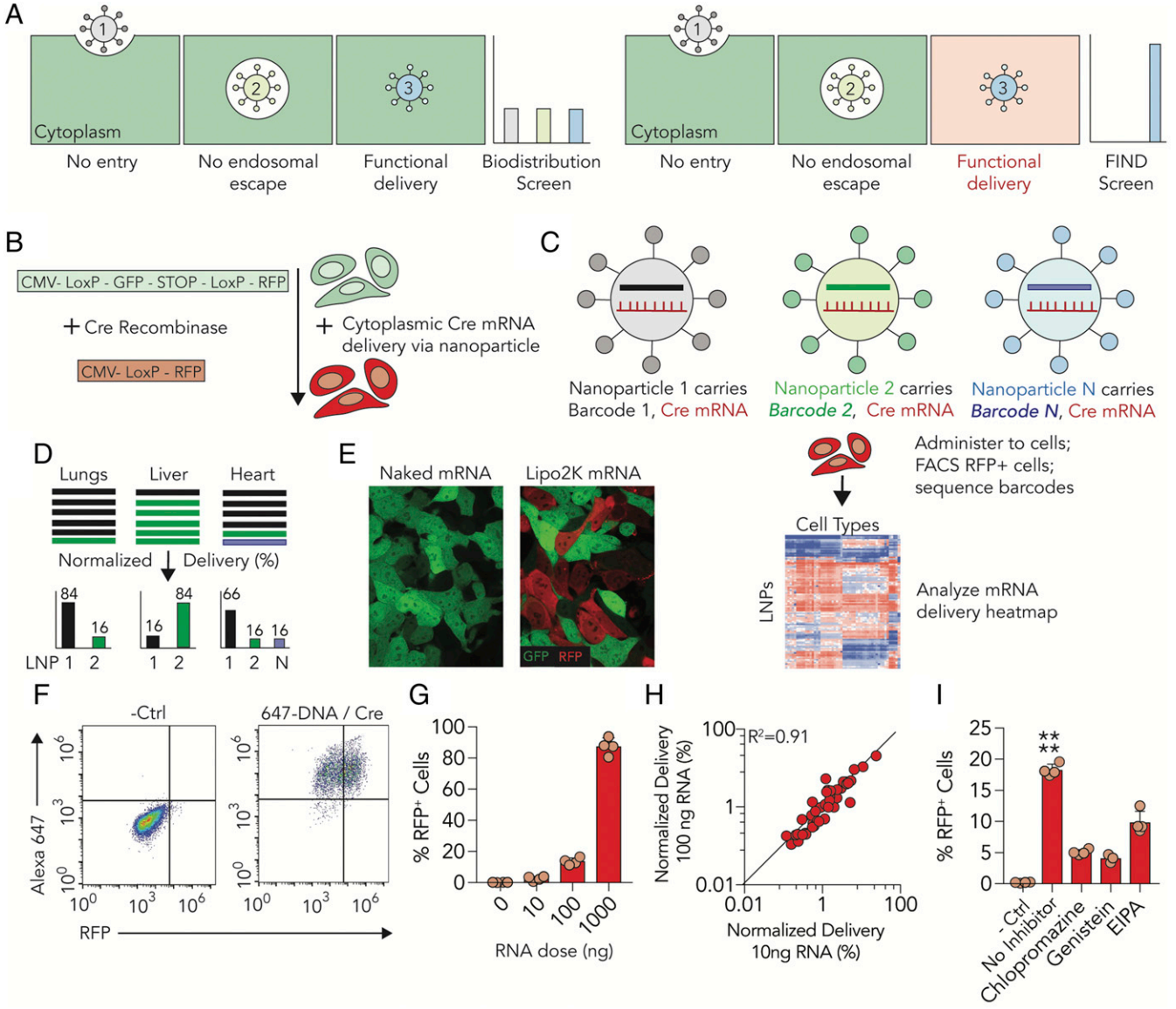

Fig. 1. FIND is a high-throughput screen for functional mRNA delivery. (*A*) Unlike previous biodistribution screens, which cannot distinguish between bound particles, particles stuck in endosomes, and particles that delivered RNA into the cytoplasm, FIND identifies LNPs that functionally deliver RNA. (*B* and *C*) Nanoparticles were formulated to carry Cre mRNA and a DNA barcode, before they were administered to Cre reporter cell lines or mice. Cells that underwent Cre-mediated genetic changes were isolated using FACS, and the DNA barcode was sequenced to identify the LNP that delivered the mRNA. (*D*) LNP barcodes were ranked by "normalized delivery"; each sample (e.g., lung 1 vs. heart 1) was analyzed individually on a single sequencing run. Using these data, we would hypothesize that LNP-1 delivered nucleic acids more efficiently to the lungs than LNP-2 and LNP-N. (*E*) LGSL-R cells were treated with naked Cre mRNA or Cre mRNA carrried by Lipofectamine 2000 (L2K). RFP expression indicates cytoplasmic Cre mRNA delivery. (*F*) Alexa 647 and RFP intensities after treatment with L2K carrying Cre mRNA and Alexa 647-labeled DNA barcode. Compared with untreated cells, there are no Alexa 647-RFP+ cells, demonstrating that biodistribution is necessary, but not sufficient, for cytoplasmic delivery. (*G*) RFP+ HEK cells as a function of the administered Cre mRNA, which was delivered with L2K. (*H*) Normalized DNA barcode delivery for 54 LNPs sequenced from RFP+ HEK cells after the administration of 10 ng or 100 ng total mRNA. A high degree of correlation between samples suggests that LNPs which deliver mRNA at the first dose deliver mRNA at the second dose. (*I*) RFP+ HEK cells following the administration of 54 LNPs (100 ng total mRNA), after cells were treated with endocytosis inhibitors. $n = 3$–4 wells per group. $^{**}P < 0.01$, $^{****}P < 0.0001$, two-tailed t test.

FACS and deep-sequenced the cells to identify LNPs that delivered mRNA. We reasoned the codelivery of mRNA and a 56-nt ssDNA could approximate the codelivery of an mRNA encoding a nuclease and guide RNA (28–30). After sequencing tdTomato$^+$ cells (Fig. 1*C*), we ranked LNPs by calculating the "normalized delivery" of each barcode. Normalized delivery is analogous to counts per million in RNA-sequencing data (Fig. 1*D* and *SI Appendix*, Fig. S1*B*). We used barcodes we previously described and validated with a number of control experiments (*SI Appendix*, Fig. S1 *C–E*) (17, 20, 21).

We characterized FIND using in vitro and in vivo experiments. First, we cultured HEK.293 cells that expressed LoxP-GFP-Stop-LoxP-RFP (LGSL-RFP) under a CMV promoter (Fig. 1*B*). These cells became RFP$^+$ 72 h after treatment with Cre mRNA carried by Lipofectamine 2000 (L2K), but not with naked Cre mRNA, which served as the negative control (Fig. 1*E* and *SI Appendix*, Fig. S1*F*). The number of RFP$^+$ cells after L2K treatment increased with dose and time, up to 3 d (*SI Appendix*, Fig. S1*G*). We then coformulated L2K with Cre mRNA and an Alexa 647-labeled DNA barcode. After 24 h, 62, 36, 2, and 0% of the cells were 647$^+$RFP$^-$, 647$^+$RFP$^+$, 647$^-$RFP$^-$, and 647$^-$RFP$^+$, respectively. This indicates that biodistribution is required, but not sufficient for functional cytosolic delivery, as we expected (Fig. 1*F*). Untreated cells—used to control for autofluorescence—were 647$^-$RFP$^-$ (Fig. 1*F* and *SI Appendix*, Fig. S1*H*).

We then formulated 54 chemically distinct LNPs (*SI Appendix*, Fig. S1 *I* and *J*) carrying Cre mRNA and a unique DNA barcode. We administered the LNPs to LGSL-RFP cells with mRNA doses of 10, 100, or 1,000 ng and an mRNA:DNA barcode mass ratio of 10:1. We observed a dose-dependent increase in RFP$^+$ cells, with over 80% of the cells RFP$^+$ 3 d after the 1,000-ng transfection (Fig. 1*G*). We sequenced barcodes at all three doses, reasoning that barcode delivery at the lowest dose (4% RFP$^+$ cells) would predict delivery at the middle dose (20% RFP$^+$ cells); we observed a strong correlation ($R^2 > 0.9$) between normalized delivery at 10-ng and 100-ng doses, suggesting this was the case (Fig. 1*H*). As a control, we sequenced cells treated with 1,000 ng mRNA; in this case, the system was saturated (>80% of the cells were RFP$^+$). As expected, the correlation between 1,000 ng and either 10 or 100 ng was weaker (*SI Appendix*, Fig. S1*K*) than the correlation between the two lower doses; importantly, these data indicate that FIND can become saturated as the percent of RFP$^+$ increases. Therefore, varying the dose by the potency of the nanoparticles pooled may be critical. We then evaluated whether the number of RFP$^+$ cells decreased after pretreatment with chlorpromazine, genistein, or ethylisopropyl amiloride (EIPA), which inhibit clathrin-, caveolin-, and macropinocytosis-mediated endocytosis, respectively. Compared with control cells that were not treated with inhibitors, RFP$^+$ cells decreased by 40–60%, recapitulating results previously obtained with individual LNPs (24, 31) (Fig. 1*I*). Taken together, these results led us to conclude that FIND could analyze mRNA delivery in vitro.

We investigated whether FIND could identify nanoparticles that deliver mRNA in vivo (Fig. 2 *A* and *B*). We formulated 112 LNPs, varying four chemical traits that influence LNP delivery in vitro: the lipid-amine compound, the molar amount of PEG, the structure of PEG, and the molar amount of cholesterol (Fig. 2*C* and *SI Appendix*, Fig. S2 *A* and *B*). Seventy-one LNPs met our two criteria for inclusion and were pooled (Fig. 2*D*). Naked DNA barcode, which should not be delivered as efficiently as DNA barcodes in LNPs, was included as a negative control. We

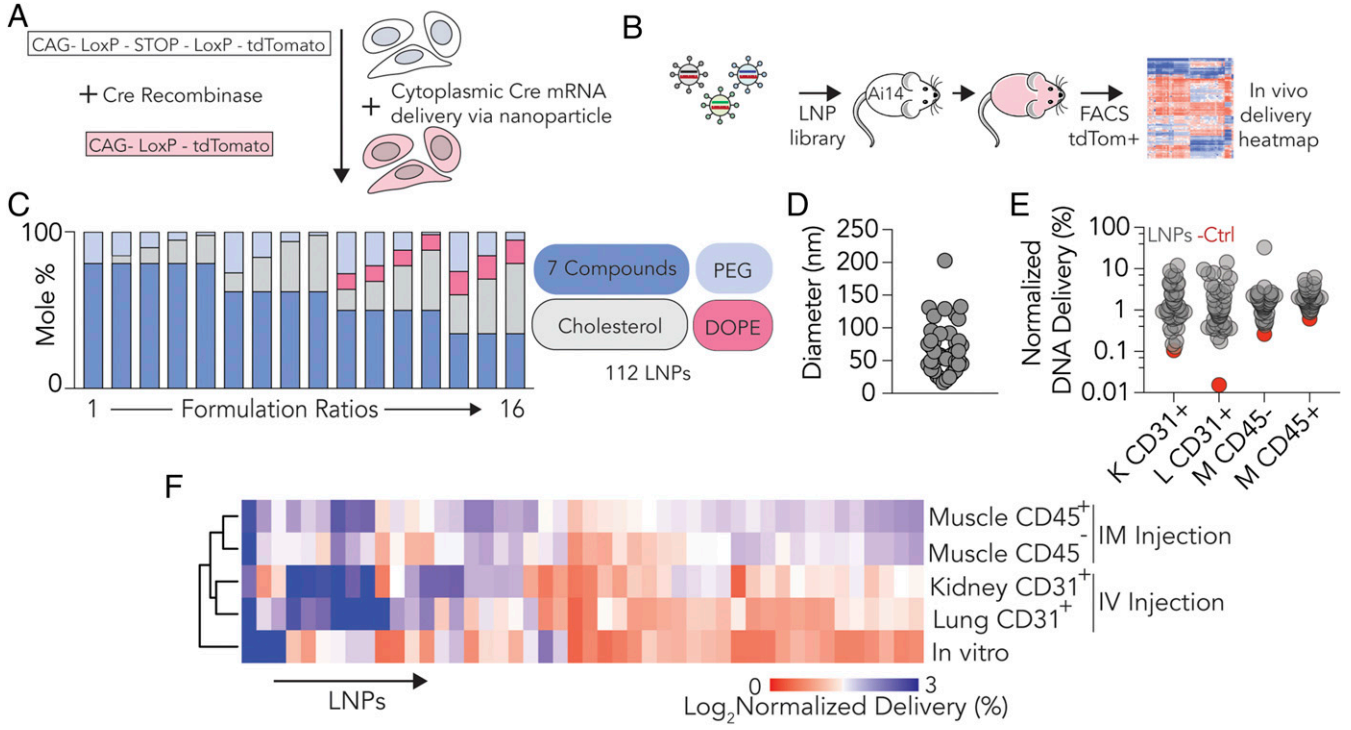

Fig. 2. FIND can quantify LNP delivery in vivo. (*A*) Cre recombinase leads to the deletion of a stop codon allowing for the expression of tdTomato driven by a CAG promoter. (*B*) Libraries of LNPs containing Cre mRNA and DNA barcodes are administered to LSL-tdTom (Ai14) mice. tdTomato+ cells are isolated by FACS and DNA barcodes are sequenced. (*C*) Screen 1 consisted of a library of 112 distinct LNPs created by formulating seven compounds with cholesterol, DOPE, and C14-PEG2000 at 16 different mole ratios. (*D*) DLS analysis of all 112 LNPs from this library; 71 formed stable LNPs and were included. (*E*) Normalized DNA delivery in kidney and lung endothelial cells (CD31+CD45–) after LNPs were i.v. injected, as well as CD45+ and CD45– cells isolated following intramuscular injection. (*F*) In vivo LNP targeting heat map generated by unbiased, Euclidean clustering. In vitro LNP delivery, in vivo intramuscular delivery, and in vivo i.v. delivery cluster separately, as expected.

i.v. injected the pooled LNPs and naked barcode into Ai14 mice at a 1.5 mg/kg total mRNA dose (average dose 0.021 mg/kg per particle). Three days later, we isolated tdTomato$^+$ lung and kidney endothelial cells (tdTomato$^+$CD31$^+$CD45$^-$). Separately, we injected 1.0 mg/kg total mRNA into mice intramuscularly and isolated immune (tdTomato$^+$CD45$^+$) and nonimmune (tdTomato$^+$CD45$^-$) cells from muscle. We gated on PBS-injected Ai14 mice for i.v. injected mice and the contralateral limb for intramuscular administration. It was important to gate on untreated Ai14 mice instead of C57BL/6J mice; gating on C57BL/6J mice could lead to inflated values of tdTomato$^+$ cells (*SI Appendix*, Fig. S2*C*). Separately, we administered the same LNPs to LGSL-RFP cells in vitro. Several lines of evidence suggested the data were robust. In all routes of administration, the naked barcode was delivered less efficiently than every LNP (Fig. 2*E*). Second, 7C1-based LNPs, which we previously optimized for in vivo RNA delivery (32), were enriched in the top 20% LNPs, compared with the other six lipid-amine compounds. (*SI Appendix*, Fig. S2 *D* and *E*). Finally, we reasoned that the route of administration would affect delivery; Euclidean clustering, a common bioinformatics technique (33) that compares how similar/dissimilar groups are to one another, and can be used to study nanoparticles in vivo (17, 20), separated intravenous, intramuscular, and in vitro delivery into three distinct clusters, as expected (Fig. 2*F*).

We formulated a second LNP library to study how PEG, cholesterol, and helper lipids [e.g., dioleoylphosphatidylethanolamine (DOPE)] influence delivery to cells in vivo. We focused on 7C1-based LNPs, since 7C1 was enriched in the first screen. We varied the PEG molar amount, as well as the alkyl length on the PEG-lipid (*SI Appendix*, Fig. S2*F*). Seventy-eight out of 108 LNPs met our two criteria for inclusion; we i.v. administered the pool to the mice at a total mRNA dose of 1.5 mg/kg. Three days later, we sequenced barcodes from tdTomato$^+$ lung and kidney endothelial cells. LNPs containing C_{14} alkyl PEG were enriched in lung endothelial cells, whereas LNPs containing C_{18} alkyl PEG were enriched in kidney endothelial cells (*SI Appendix*, Fig. S2 *G* and *H*). To validate the relationship between lung delivery, kidney delivery, and PEG structure, we formulated a third LNP library. We formulated 158 LNPs designed to improve lung delivery relative to kidney delivery by only using C_{14} alkyl-tail PEG varying helper lipid composition (*SI Appendix*, Fig. S2*I*). We found 3.75 times more lung endothelial cells were tdTomato$^+$ than kidney endothelial cells, a ratio that was significantly higher than the second screen (*SI Appendix*, Fig. S2*J*), as expected. Consistent with previous results (17, 20), we did not observe a relationship between LNP size and delivery to endothelial cells between the range of 20–200 nm (*SI Appendix*, Fig. S2*K*). The poor performance of the naked barcode, enrichment of 7C1, the fact that unbiased clustering separated the three routes of administration, and the PEG data convinced us FIND was capable of quantifying delivery in vivo.

After completing these in vitro and in vivo validation experiments, we selected two LNPs (named 7C2 and 7C3) for more thorough characterization (Fig. 3 *A* and *B* and *SI Appendix*, Fig. S3 *A* and *B*). The 7C2 was formulated with 7C1:cholesterol:C14-PEG2000:18:1 Lyso PC at a molar ratio of 50:23.5:6.5:20. The 7C3 was formulated with 7C1:cholesterol:C14-PEG2000:DOPE at a molar ratio of 60:10:25:5. The 7C2 and 7C3 formed stable LNPs with average diameters between 50 and 80 nm when formulated with siRNA, single-guide RNA (sgRNA), or mRNA (*SI*

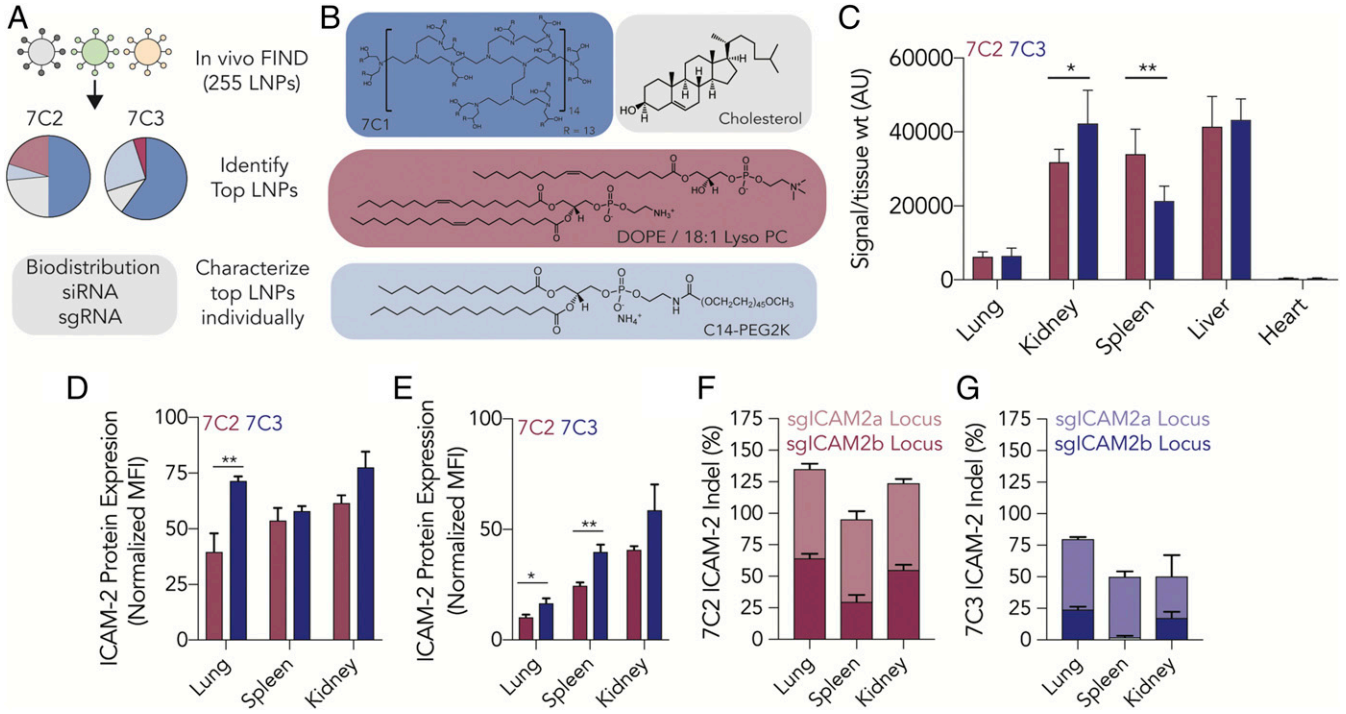

Fig. 3. Characterization of lead nanoparticles discovered by FIND. (*A*) The top two particles, 7C2 and 7C3, discovered following three rounds of FIND are characterized by measuring biodistribution, delivery of siRNA, sgRNA. (*B*) The 7C2 and 7C3 were composed of 7C1 compound, cholesterol, C14-PEG2000, and helper lipids, 18:1 Lyso PC and DOPE, respectively. (*C*) Following a 0.75-mg/kg Barcode-Cy5.5 administration, biodistribution of 7C2 and 7C3 was quantified and normalized to tissue weight. $n = 4$ miceper group. $^*P < 0.05$, $^{**}P < 0.01$, two-way ANOVA. (*D*) Following a 1-mg/kg siICAM2 administration, both 7C2 and 7C3 induced ICAM2 protein silencing in endothelial cells by flow cytometry. The 7C2 demonstrates more robust protein silencing in lung endothelial cells than 7C3. $n = 4$ mice per group. $^{**}P < 0.01$, two tailed t test. (*E*–*G*) Following repeat administration of 7C2 and 7C3 at 1.5 mg/kg sgICAM2a and sgICAM2b, ICAM2 (*E*) protein and (*F* and *G*) indels were measured in endothelial cells isolated from multiple organs using FACS. $n = 3$–4 mice per group. $^*P < 0.05$, $^{**}P < 0.01$, two-tailed t test.

Appendix, Fig. S3 *C* and *D*). The in vitro endocytosis and functional Cre mRNA delivery of both LNPs in LGSL-RFP cells decreased by at least 40% when cells were pretreated with chlorpromazine and genistein, relative to cells that were not treated with inhibitors. EIPA impacted LNP uptake but did not significantly decrease functional delivery in vitro (*SI Appendix*, Fig. S3 *E–H*). These results suggest 7C2 and 7C3 are endocytosed in vitro via several pathways. To study biodistribution, 7C2 and 7C3 were formulated with a Cy5.5-conjugated DNA barcode and i.v. injected into separate mice at a dose of 0.75 mg/kg DNA. Three hours later—a time point that is sufficiently long for LNPs to be cleared from the blood (34)—Cy5.5 ex vivo fluorescence, normalized by tissue weight, was highest in the spleen, kidney, and liver, suggesting 7C2 and 7C3 distributed to these tissues (Fig. 3*C* and *SI Appendix*, Fig. S3*I*).

We tested whether 7C2 and 7C3 functionally delivered siRNA, sgRNA, and mRNA, which are all clinically relevant. We performed our individual LNP proof-of-concept experiments with nucleic acids targeting ICAM-2. We chose this target for three reasons. First, ICAM-2 is related to a number of inflammatory diseases (35, 36). Second, ICAM-2 expression is robust on endothelial cells. Third, there is a well-validated monoclonal antibody to ICAM-2, which allows us to quantify protein expression robustly using FACS.

First, we formulated the LNPs to carry siRNA targeting ICAM-2. Three days after i.v. injecting mice with PBS, 2.0 mg/kg siGFP (a higher dose was used to test tolerability), or 1.0 mg/kg siICAM-2, we quantified ICAM-2 protein mean fluorescent intensity (MFI) in lung, kidney, and splenic endothelial cells using flow cytometry (32, 37). Both siRNAs were previously validated and chemically modified to reduce immunostimulation and promote on-target mRNA degradation (32, 37) (*SI Appendix*, Fig. S3*J*). ICAM-2 MFI was constant in PBS- and siGFP-treated mice but decreased by 60% in lung endothelial cells isolated from mice injected with siICAM-2. The 7C2-mediated delivery of siRNA reduced ICAM-2 expression in lung endothelial cells more than in splenic endothelial cells, whereas 7C3 silencing was more robust in splenic endothelial cells (Fig. 3*D* and *SI Appendix*, Fig. S3*K*). Compared with PBS-treated mice, mice injected with 2.0 mg/kg siGFP did not show any weight loss or changes in organ weight (*SI Appendix*, Fig. S3 *L–N*).

We then quantified 7C2- and 7C3-mediated sgRNA delivery. We coformulated two sgRNAs that were chemically modified at the 5′ and 3′ termini (38) and injected each at a dose of 0.75 mg/kg into mice that constitutively express SpCas9 (39) (*SI Appendix*, Fig. S3*O*). After three injections, ICAM-2 MFI decreased by up to 90, 75, and 59% in lung, spleen, and kidney endothelial cells, respectively for 7C2 (Fig. 3*E*). To confirm protein silencing was mediated by gene editing, we measured (40) ICAM-2 insertions and deletions (indels) in lung, spleen, and kidney endothelial cells and found between 30 and 70% editing per locus, leading to overall ICAM-2 indel percentages of 135, 95, and 123% indel, respectively for 7C2 (Fig. 3 *F* and *G* and *SI Appendix*, Fig. S3 *P* and *Q*). In these experiments, we utilized two sgRNAs per gene; thus, the total indel percentage was 200% (100% per site). Compared with PBS mice, mice treated with LNPs did not lose weight (*SI Appendix*, Fig. S3 *R* and *S*). Based on these experiments, we concluded that 7C2 potently delivered small RNAs to pulmonary endothelial cells in vivo.

In our siRNA and sgRNA experiments, 7C2 outperformed 7C3 and potently delivered RNAs to pulmonary endothelial cells. We then investigated whether the same observations were true for the delivery of large RNAs (mRNA). We formulated 7C2 and 7C3 to carry Cre mRNA and injected the LNPs into separate mice at a dose of 1.5 mg/kg mRNA (Fig. 4*A*). Three days later, we isolated tdTomato$^+$ immune cells and endothelial cells from the spleen, kidney, heart, lung, and liver, as well as hepatocytes. We made two interesting observations. First, contrasting the small RNA delivery experiments, 7C3 outperformed 7C2. Second, splenic endothelial cells were targeted efficiently (Fig. 4*B*). Notably, relative to splenic endothelial cells, very few immune cells and hepatocytes were tdTomato$^+$ (*SI Appendix*, Fig. S3 *T* and *U*). Given this degree of specificity has not been reported to date, we repeated the experiment using 34 Ai14 mice over the course of several months. The 7C3 delivered Cre mRNA to splenic endothelial cells in every experiment (Fig. 4*C*). However, we did observe batch-to-batch variability with respect to hepatocyte targeting (Fig. 4 *C* and *D*). In 22 of the 34 mice, a low percentage of hepatocytes were tdTomato$^+$ (<13%); in 12 of the 34 mice, we observed high percentages of tdTomato$^+$ cells. Averaging data from all 34 mice, the number of tdTomato$^+$ splenic endothelial cells (43%) was 2.2 times higher than the number of tdTomato$^+$ hepatocytes (20%) (Fig. 4*D*). Splenic endothelial cell delivery was also dose-dependent (*SI Appendix*, Fig. S3*V*). The variable delivery to hepatocytes was unlikely to be driven by toxicity; throughout our studies, we injected 34 mice with 7C3 and did not observe changes in mouse weight or obvious signs of toxicity (*SI Appendix*, Fig. S3*W*). We were unable to identify the source of batch variability; however, we hypothesize it is driven by the polymeric backbone of 7C3 and the resulting heterogenous chemical structure. Our data strongly suggest that future FIND screens should focus on compounds with defined chemical structures, which may be less likely to exhibit biological heterogeneity. The data also demonstrate that 7C3 can efficiently deliver mRNA to splenic endothelial cells in vivo. Importantly, the 7C2 and 7C3 formulations both included the lipomer 7C1 but had variable molar compositions of helper lipids (18:1 Lyso PC and DOPE), which distinguished them chemically from previously described endothelial-targeting nanoparticles. The differences in delivery between 7C2 and 7C3 provide interesting preliminary evidence that suggests changing the composition of helper lipids added to a given ionizable amine can alter tropism. The compositions and efficacy of 7C2 and 7C3 are included in *SI Appendix*, Fig. S4.

Given the difference between small and large RNA delivery, we quantified how LNPs codelivered CRISPR-Cas9 mRNA and sgRNA. We formulated Cas9 mRNA and two guides targeting ICAM-2 into LNPs at a 3:1 mass ratio and injected a 2.0 mg/kg total i.v. on day 0 and 2. On day 7, we isolated endothelial cells from the spleen, lung, kidney, and liver, as well as hepatocytes (*SI Appendix*, Fig. S5*A*). Splenic endothelial cell editing mediated by 7C3 was more robust than editing in hepatocytes (*SI Appendix*, Fig. S5*B*). Mice injected with 7C2 and 7C3 did not lose weight, compared with PBS-treated mice (*SI Appendix*, Fig. S5*C*). These studies were also conducted with sgRNAs that were chemically modified at the 5′ and 3′ termini (38); during the course of the experiments, two groups demonstrated that heavily modified sgRNAs improved in vivo editing (7, 8). We redesigned sgICAM2b with "enhanced" modifications (8) (referred to as e-sgICAM2) (*SI Appendix*, Fig. S5*D*) and formulated 7C3 to carry Cas9 mRNA and e-sgICAM2. Given that e-sgICAM2 was more likely to resist degradation in vivo (8), we hypothesized that the optimal mass ratio of Cas9 mRNA:sgRNA would decrease from 3:1, which is the optimized ratio with minimally stablized sgRNAs. To test this, we formulated 7C3 with Cas9 mRNA:e-sgRNA ratios of 5:1, 3:1, and 1:1, keeping the total injected dose constant at 2.0 mg/kg. After injecting mice i.v. with 2.0 mg/kg total RNA (Cas9 mRNA + sgRNA) on days 0 and 2, we isolated splenic endothelial cells and hepatocytes using FACS on day 7. We observed gene editing in splenic endothelial cells and hepatocytes at all mRNA-to-sgRNA ratios, with an average of 20% editing in the 1:1 mass ratio group (Fig. 4 *E* and *F*). As expected, the lower Cas9 mRNA:e-sgRNA mass ratio led to increased editing. Once again, mice injected with 7C3 did not lose weight compared with PBS-treated controls (*SI Appendix*, Fig. S5*E*). This is a demonstration of systemic Cas9-mediated editing of

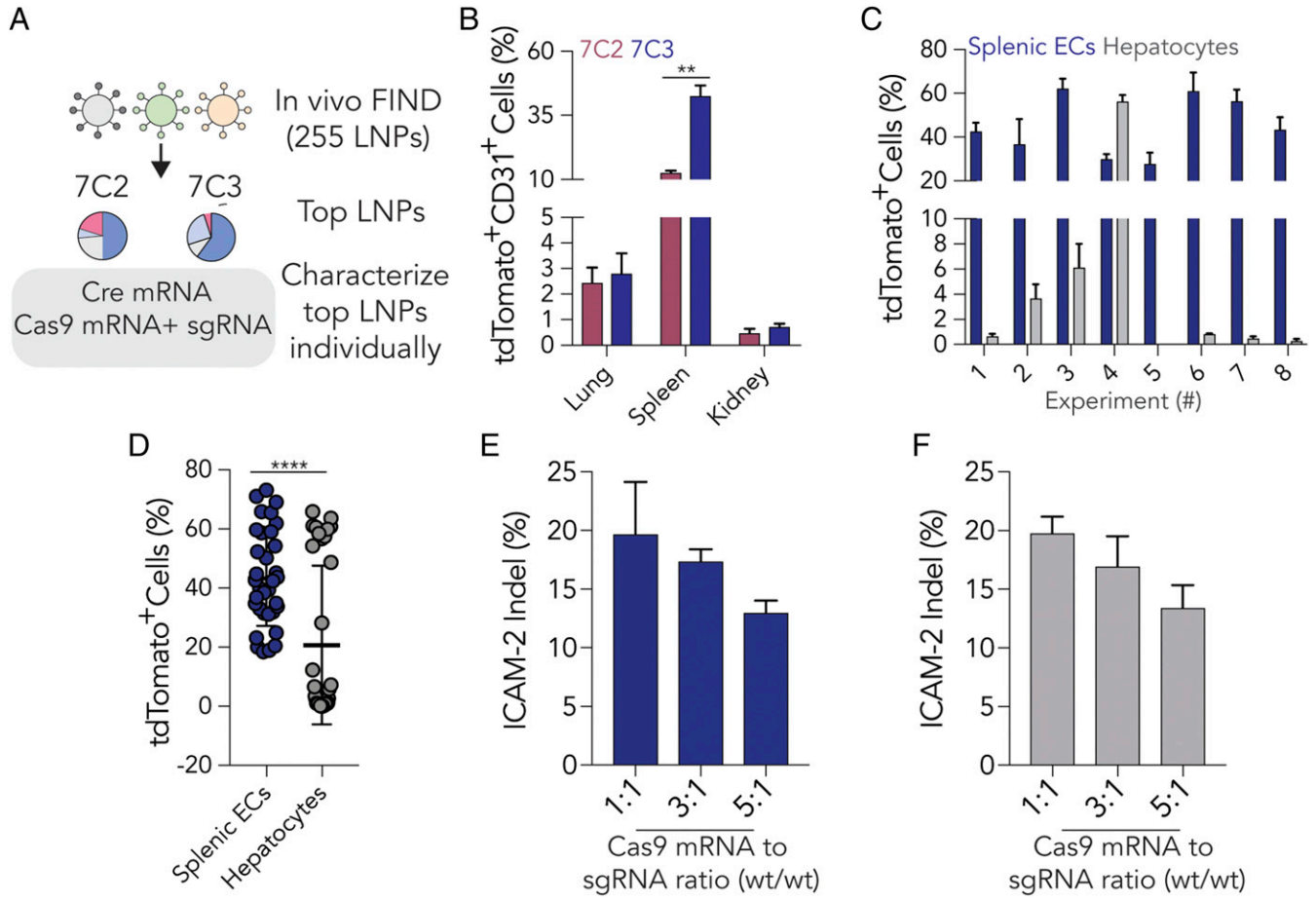

Fig. 4. (*A*) The top two particles, 7C2 and 7C3, are characterized by delivery of Cre mRNA and codelivery of Cas9 mRNA and sgRNA. (*B*) Percentage of tdTomato+ endothelial cells in LSL-Tom mice 72 h after a single 1.5-mg/kg injection of Cre mRNA delivered by 7C2 or 7C3. $n = 4$ mice per group. $^{**}P < 0.01$, two-tailed *t* test. (*C*) Percentage of tdTomato+ splenic endothelial cells and hepatocytes in LSL-Tom mice following a single 1.5-mg/kg injection of Cre mRNA delivered by 7C3 from eight independent experiments representing 34 mice. (*D*) Percentages from all eight experiments of tdTomato+ splenic endothelial cells and hepatocytes in LSL-Tom mice following a single 1.5-mg/kg injection of Cre mRNA delivered by 7C3. $n = 34$. $^{****}P < 0.0001$, two-tailed *t* test. (*E*) Indel percentage in splenic ECs following two injections of 7C3 carrying Cas9 mRNA and e-sgICAM2 at a mass ratio of 1:1, 3:1, and 5:1. (*F*) Indel percentage in hepatocytes following two injections of 7C3 carrying Cas9 mRNA and e-sgICAM2 at a mass ratio of 1:1, 3:1, and 5:1.

endothelial cells in wild-type mice. These data demonstrate that systemically administered nanoparticles can edit endothelial cells, and that the ideal Cas9:sgRNA ratio will depend on the relative stability of the two molecules.

Discussion

FIND is a high-throughput method to quantify functional mRNA delivery mediated by LNPs. The distinction between biodistribution and functional delivery is significant; >96% of delivered RNA does not escape the endosome (23, 24), and endosomal escape may vary with cell type or disease state (41), making it hard to predict functional delivery using biodistribution. Notably, Cre mRNA must be translated in the cytoplasm, translocate into the nucleus, and edit target DNA. The similarity between these steps and the steps required for nuclease-mediated gene editing is one reason we selected a Cre-based FIND system. We also chose the Cre-lox system because Ai14 mice are well-validated and commonly available (27). Moreover, the Cre-mediated signal is strong and does not vary dramatically with time; by contrast, a GFP-based system would have a signal that varies hour by hour, making FACS gates impossible to interpret during a long experimental day.

Although we focused on endothelial cells, FIND is agnostic to cell type; we envision FIND studies that identify LNPs targeting other cells. Ai14 mice have recently been used to monitor LNP-mediated delivery to immune populations at a cellular resolution (42). Given that on- and off-target cells can be isolated from the same mouse, FIND may also be used to identify (or iteratively evolve) LNPs with high therapeutic windows. To further increase the ratio of splenic endothelial cell:hepatocyte delivery, we could incorporate endothelial-cell-targeting ligands (43, 44).

More generally, this ability to study how hundreds of LNPs target combinations of cells in vivo may elucidate relationships between LNP structure and in vivo functional delivery. In this case, FIND enabled us to quickly identify two lead LNPs. Here we delivered sgRNAs targeting the inflammation-related gene ICAM-2. However, the long-term utility of FIND will be defined by its ability to identify nanoparticles for in vivo gene editing more efficiently than the current gold standard, which is in vitro screening. Relatedly, to fully utilize the large in vivo datasets generated by FIND, efforts will need to be made to develop high-throughput ways of characterizing LNP characterizations zeta-potential, pK_a, and lipid bilayer structure. We believe that, in time, these advances will help position FIND to help facilitate the discovery of structure–activity relationships to nonliver tissues. In future studies, it will also be important to further improve the efficiency of gene editing in endothelial cells beyond 20%.

We did not observe noticeable experimental variability within a given FIND screening experiment. We quantified the consistency of the sequencing readouts by analyzing the normalized DNA delivery values between bioreplicates. In all cell types, in each of the three screens, there were no overt differences between bioreplicates, suggesting the precision of the sequencing was high (*SI Appendix*, Fig. S6). In individual LNP testing, we did observe variability in hepatocyte delivery when 7C3 was administered over several batches to a total of 34 mice. Notably, delivery to splenic ECs was consistent, as was the (lack of) delivery to all other tested cell types. We were unable to identify the chemical variations that led to batch variability in hepatocyte targeting. Two possibilities that will require further investigation include variable LNP chemical structure and variable mRNA activity. Performing FIND screens with well-defined compounds could minimize batch-to-batch variability.

We note that when testing many new LNPs batch variability may be observed since the formulations are not yet optimized. However, this issue is not related to FIND or to pooled LNP screens; it is just as likely to occur when LNPs are tested individually. We believe FIND may actually minimize unwanted error in two ways. First, Cre-based reporters quantify delivery at the level of cell type. Identifying the cell type with batch issues is much easier than with two common approaches used in the field today: mRNA encoding luciferase or erythropoietin, which quantifies protein production at the tissue- and organism-level, respectively. Second, when nanoparticles are screened individually, missed injections, small changes in time points, mouse age, and other variables can introduce "silent" experimental variability that affects how LNP1 performs, relative to LNP2. Here, we inject all of the nanoparticles into the same mouse, which helps to reduce these sources of unintentional experimental variance. At the same time, FIND has several important limitations. LNPs must be stable and must be well-tolerated. Like all DNA-based screens, it is imperative to prevent DNA contamination.

Finally, we note that the doses of mRNA or gene editing constructs that are well-tolerated after systemic administration to patients has not yet been established. In one related example, the FDA approved ONPATTRO therapeutic, which is an siRNA systemically administered in an LNP, at a dose of 0.3 mg/kg. This may provide an initial estimate of the mRNA doses that are tolerated in the clinic. However, Cas9 mRNA is >100 times larger than a single siRNA duplex (~4,500-nt ssRNA vs. 21-nt dsRNA). As a result, there is still a need to further improve the potency of the drug delivery systems as well as the mRNA drugs to advance novel Cas9 therapies into the clinic. Despite these caveats, FIND is a robust method to quantify how hundreds of LNPs deliver mRNA to any combination of cell types in vivo. We believe FIND is well-positioned to help identify LNPs with novel tropisms, which could lead to improved nonliver RNA drugs.

Materials and Methods

Nanoparticle Formulation. Nanoparticles were formulated using a microfluidic device as previously described (26). Briefly, nucleic acids (mRNA, DNA barcodes, siRNA, and sgRNA) were diluted in 10 mM citrate buffer (Teknova) while lipid-amine compounds, alkyl-tailed PEG, cholesterol, and helper lipids were diluted in ethanol. For nanoparticle screens, Cre mRNA and DNA barcodes were mixed at a 10:1 mass ratio. Citrate and ethanol phases were combined in a microfluidic device by syringes (Hamilton Company) at a flow rate of 600 μL/min and 200 μL/min, respectively. All PEGs, cholesterol, and helper lipids were purchased from Avanti Lipids.

DNA Barcoding. Each chemically distinct LNP was formulated to carry its own unique DNA barcode (Fig. 1). For example, LNP1 carried DNA barcode 1, while the chemically distinct LNP2 carried DNA barcode 2. DNA barcodes were designed rationally with several characteristics, as we previously described (20). Fifty-six- nucleotide-long ssDNA sequences were purchased from Integrated DNA Technologies. The two nucleotides on the 5′ and 3′ ends of the 56-nt ssDNA were modified with phosphorothioates to reduce exonuclease degradation and improve DNA barcode stability. To ensure equal amplification of each sequence, we included universal forward and reverse primer regions on all barcodes. To monitor for PCR bias, each barcode was also designed with seven random nucleotides. Each barcode was distinguished using a unique 8-bp sequence. An 8-bp sequence can generate over 4^8 (65,536) distinct barcodes. We used 240 distinct 8-bp sequences designed by to prevent sequence bleaching on the Illumina MiniSeq sequencing machine.

Nanoparticle Characterization. LNP hydrodynamic diameter was measured using high-throughput DLS (DynaPro Plate Reader II; Wyatt). LNPs were diluted in sterile 1× PBS to a concentration of ~0.06 μg/mL and analyzed. To avoid using unstable LNPs, and to enable sterile purification using a 0.22-μm filter, LNPs were included only if they met three criteria: diameter >20 nm, diameter <200 nm, and correlation function with one inflection point. Particles that met these criteria were dialyzed with 1× PBS (Invitrogen) and were sterile-filtered with a 0.22-μm filter.

Cell Culture. In vitro experiments were performed using HEK.293 cells (GenTarget) stably transduced with a CMV-lox-GFP-stop-lox-RFP construct cultured in DMEM/F-12 50/50 media (Corning) supplemented by 10% (vol/vol) FBS (VWR) and 1% (vol/vol) penicillin–streptomycin (VWR). Cells were seeded in a six-well plate at a density of 300,000 cells per well; 24 h later, LNPs were added with a total mRNA dose of 100 ng. Six hours after transfection, media was refreshed. DNA was isolated using 50 μL of QuickExtract (EpiCentre).

Endocytosis Inhibition. For experiments shown in Fig. 1 and *SI Appendix*, Fig. S3 *E–H*, cells were incubated with endocytosis inhibitors. Specifically, 1 h before incubation with pooled LNPs, inhibitors of clathrin-mediated endocytosis (chlorpromazine, 100 μM; Alfa Aesar), caveolae-mediated endocytosis (genistein, 100μM; TCI America), and macropinocytosis [5-(*N*-Ethyl-*N*-isopropyl) Amiloride, EIPA, 50 μM; Toronto Research Chemicals] were added to cells.

Animal Experiments. All animal experiments were performed in accordance with the Georgia Institute of Technology's Institutional Animal Care and Use Committee. LSL-Tomato (007914), C57BL/6J (000664), and constitutive SpCas9 (026179) mice were purchased from The Jackson Laboratory and used between 5–12 wk of age. In all experiments, we used $n = 3$–5 mice per group. Mice were injected i.v. via the lateral tail vein or intramuscularly into the quadriceps, tibialis anterior, and gastrocnemius. The nanoparticle concentration was determined using NanoDrop (Thermo Scientific). For in vivo nanoparticle screens, mice were administered 1.5 mg/kg for intravascular and 1 mg/kg for intramuscular administration. The dosing schedule for each experiment is shown in *SI Appendix*, Fig. S7.

Cell Isolation and Staining. Cells were isolated 72 h after injection with LNPs unless otherwise noted. Mice were perfused with 20 mL of 1× PBS through the right atrium. Tissues were finely cut and then placed in a digestive enzyme solution with collagenase type I (Sigma-Aldrich), collagenase XI (Sigma-Aldrich), and hyaluronidase (Sigma-Aldrich) at 37 °C at 550 rpm for 45 min. The digestive enzyme for heart and spleen included collagenase IV (32, 37, 45). Cell suspension was filtered through 70-μm mesh and red blood cells were lysed. Cells were stained to identify specific cell populations and sorted using the BD FacsFusion and BD Facs Aria IIIu cell sorters in the Georgia Institute of Technology Cellular Analysis Core. For in vitro experiments, BD Accuri C6 and BD FacsFusion were used. The antibody clones used were anti-CD31 (390; BioLegend), anti-CD45.2 (104; BioLegend), and anti-CD102 (3C4; BioLegend). PE anti-mCD47 (miap301; BioLegend) was used for tdTomato compensation. Representative flow gates are located in *SI Appendix*, Fig. S8. PBS-injected Ai14 mice were used to gate tdTomato populations for i.v. administration, while contralateral limbs were used to gate for intramuscular experiments.

Biodistribution. LNPs encapsulating Cy5.5-tagged DNA barcode were administered at 0.75 mg/kg. After 3 h, tissues were isolated without perfusion, weighed individually, and imaged using the Licor Odyssey CLx imaging system. Signal intensity was normalized to tissue weight.

Endothelial RNA interference. C57BL/6J mice were injected with 7C2 and 7C3 with PBS, 2 mg/kg siCTRL (siGFP-647) (AxoLabs), or 1 mg/kg siICAM2 (AxoLabs). In all cases, siRNAs were chemically modified at the 2′ position to increase stability and negate immunostimulation. Both siGFP and siICAM2 sequences have been previously reported several times (32, 37, 45).

Seventy-two hours after injection, tissues were isolated and protein expression was determined via flow cytometry. ICAM2 MFI in PBS-treated mice was normalized to 100%, and all treated groups were compared with this control group.

Endothelial Gene Editing. Mice constitutively expressing SpCas9 were injected three times with 7C2 or 7C3 carrying 1.5 mg/kg of two chemically modified sgRNAs with thee nucleotides modified on the 5′ and 5′ ends (TriLink Biotechnologies) targeting ICAM2 (sgICAM2ab) (1:1 mass ratio). Separately, C57BL/6J mice were injected two times with 2 mg/kg with 7C2 and 7C3 formulated to carry both SpCas9 mRNA (L-7206; Trilink Biotechnology) and sgICAM2ab at a 3:1 mass ratio. Five days after the last injection, tissues were isolated, and ICAM2 protein expression was measured concurrently while ∼20,000 cells were sorted into QuickExtract. Next, C57BL/6J mice were injected two times with 2 mg/kg with 7C3 formulated to carry both SpCas9 mRNA (L-7206; Trilink Biotechnology) and e-sgICAM2 (AxoLabs) at a 1:1, 3:1, and 5:1 mass ratio. Five days after the last injection, tissues were isolated, and ICAM2 protein expression was measured concurrently while ∼20,000 cells were sorted into QuickExtract. Indel formation was measured by TIDE (https://www.deskgen.com/landing/tide.html).

Tissue Immunostaining. Excised organs were fixed overnight in 4% paraformaldehyde (Electron Microscopy Systems) in PBS. Tissues were washed twice in PBS and cryoprotected in 30% sucrose in PBS until the organs sank to the bottom of the container. Organs were then embedded in optimal cutting temperature compound (Tissue-Tek) and cryosectioned (10 μm) onto slides. Antigen retrieval was performed on slides for 10 min in a pressure cooker using low-pH antigen-retrieval solution (Life Technologies). Sections were then permeabilized with 0.2% Triton X-100 (Sigma-Aldrich) in PBS for 10 min at room temperature (RT) before being blocked for nonspecific binding with 5% donkey serum (Sigma-Aldrich) in PBS for 1 h at RT. Sections were incubated with anti-VE cadherin (BV13; Biolegend), diluted to 0.5 μg/mL in PBS, overnight at 4 °C. After three washes with PBS, sections were incubated at RT with Alexa Flour 647 conjugated donkey anti-rat (Thermo Fisher) diluted in PBS for 2 h. After two PBS washes, nuclei were stained with DAPI (Life Technologies), and coverslips were mounted using Prolong Gold (Life Technologies).

Microscopy. Images were acquired with a Hamamatsu Flash 4.0 v2 sCMOS camera on a PerkinElmer UltraView spinning disk confocal microscope mounted to a Zeiss Axiovert 200M body. Single-cell images were acquired using Volocity (PerkinElmer) with Z-stacks taken in 0.2-μm increments with a 63× N.A. 1.4 plan-apochromat objective. Stitched images were acquired using a 20× N.A. 0.8 objective with an automated XY stage (ASI) controlled by Volocity and set to 20% overlap. All images were linearly contrast enhanced.

PCR Amplification. All samples were amplified and prepared for sequencing using a one-step PCR protocol as previously described (20). More specifically, 1 μL of primers (5 μM for final reverse/forward, 0.5 μM for base forward) were added to 5 μL of Kapa HiFi 2× master mix, and 4 μL template DNA/water. The reaction was run for 30 cycles. When the PCR did not produce clear bands, the primer concentrations, DNA template input, PCR temperature, and number of cycles were optimized for individual samples.

Deep Sequencing. Illumina deep sequencing was conducted in Georgia Institute of Technology's Molecular Evolution core. Runs were performed on an Illumina Miniseq. Primers were designed based on Nextera XT adapter sequences.

Data Normalization. Counts for each particle, per tissue, were normalized to the barcoded LNP mixture we injected into the mouse. This "input" DNA provided the DNA counts and was used to normalize DNA counts from the cells and tissues.

Data Analysis and Statistics. Sequencing results were processed using a custom Python-based tool to extract raw barcode counts for each tissue. These raw counts were then normalized with an R script prior for further analysis. Statistical analysis was done using GraphPad Prism 7; more specifically, one-tailed *t* test or one-way ANOVAs were used where appropriate. Data are plotted as mean ± SEM unless otherwise stated.

ACKNOWLEDGMENTS. We thank Jordan Cattie, Taylor E. Shaw, Timothy Mark O'Shea, Sommer Durham, and the Georgia Institute of Technology Cellular Analysis and Cytometry core. C.D.S., K.P., and J.E.D. were supported by Georgia Tech startup funds (to J.E.D.) This work was also supported by NIH/National Institute of General Medical Sciences (NIGMS)-sponsored Immunoengineering Training Program Grant T32EB021962 (to C.D.S.), Georgia Research Assistantship Grant 3201330 (to C.M.M.), NIH/NIGMS-sponsored Cell and Tissue Engineering (CTEng) Biotechnology Training Program Grant T32GM008433 (to K.P. and S.E.A.), and National Institutes of Health GT BioMAT Training Grant 5T32EB006343 (to M.G.C.). Research was funded by Cystic Fibrosis Research Foundation Grant DAHLMA15XX0 (to J.E.D.), Parkinson's Disease Foundation Grant PDF-JFA-1860 (to J.E.D.), and the Bayer Hemophilia Awards Program AGE DTD (J.E.D.). This content is solely the responsibility of the authors and does not necessarily represent the official views of the NIH.

1. Coelho T, et al. (2013) Safety and efficacy of RNAi therapy for transthyretin amyloidosis. *N Engl J Med* 369:819–829.
2. Adams D, et al. (2018) Patisiran, an RNAi therapeutic, for hereditary transthyretin amyloidosis. *N Engl J Med* 379:11–21.
3. Rizk M, Tüzmen Ş (2017) Update on the clinical utility of an RNA interference-based treatment: Focus on Patisiran. *Pharm Genomics Pers Med* 10:267–278.
4. Bahl K, et al. (2017) Preclinical and clinical demonstration of immunogenicity by mRNA vaccines against H10N8 and H7N9 influenza viruses. *Mol Ther* 25:1316–1327.
5. Miller JB, et al. (2017) Non-Viral CRISPR/Cas gene editing in vitro and in vivo enabled by synthetic nanoparticle co-delivery of Cas9 mRNA and sgRNA. *Angew Chem Int Ed Engl* 56:1059–1063.
6. Jiang C, et al. (2017) A non-viral CRISPR/Cas9 delivery system for therapeutically targeting HBV DNA and pcsk9 in vivo. *Cell Res* 27:440–443.
7. Yin H, et al. (2017) Structure-guided chemical modification of guide RNA enables potent non-viral in vivo genome editing. *Nat Biotechnol* 35:1179–1187.
8. Finn JD, et al. (2018) A single administration of CRISPR/Cas9 lipid nanoparticles achieves robust and persistent in vivo genome editing. *Cell Rep* 22:2227–2235.
9. Lee B, et al. (2018) Nanoparticle delivery of CRISPR into the brain rescues a mouse model of fragile X syndrome from exaggerated repetitive behaviours. *Nat Biomed Eng* 2:497–507.
10. Lee K, et al. (2017) Nanoparticle delivery of Cas9 ribonucleoprotein and donor DNA *in vivo* induces homology-directed DNA repair. *Nat Biomed Eng* 1:889–901.
11. Gao X, et al. (2018) Treatment of autosomal dominant hearing loss by in vivo delivery of genome editing agents. *Nature* 553:217–221.
12. Zuris JA, et al. (2015) Cationic lipid-mediated delivery of proteins enables efficient protein-based genome editing in vitro and in vivo. *Nat Biotechnol* 33:73–80.
13. Tsoi KM, et al. (2016) Mechanism of hard-nanomaterial clearance by the liver. *Nat Mater* 15:1212–1221.
14. Zhang YN, Poon W, Tavares AJ, McGilvray ID, Chan WCW (2016) Nanoparticle-liver interactions: Cellular uptake and hepatobiliary elimination. *J Control Release* 240:332–348.
15. Augustin HG, Koh GY (2017) Organotypic vasculature: From descriptive heterogeneity to functional pathophysiology. *Science* 357:eaal2379.
16. Whitehead KA, et al. (2014) Degradable lipid nanoparticles with predictable in vivo siRNA delivery activity. *Nat Commun* 5:4277.
17. Paunovska K, et al. (2018) A direct comparison of in vitro and in vivo nucleic acid delivery mediated by hundreds of nanoparticles reveals a weak correlation. *Nano Lett* 18:2148–2157.
18. Love KT, et al. (2010) Lipid-like materials for low-dose, in vivo gene silencing. *Proc Natl Acad Sci USA* 107:1864–1869.
19. Semple SC, et al. (2010) Rational design of cationic lipids for siRNA delivery. *Nat Biotechnol* 28:172–176.
20. Dahlman JE, et al. (2017) Barcoded nanoparticles for high throughput in vivo discovery of targeted therapeutics. *Proc Natl Acad Sci USA* 114:2060–2065.
21. Paunovska K, et al. (2018) Analyzing 2000 in vivo drug delivery data points reveals cholesterol structure impacts nanoparticle delivery. *ACS Nano* 12:8341–8349.
22. Lokugamage MP, Sago CD, Dahlman JE (2018) Testing thousands of nanoparticles in vivo using DNA barcodes. *Curr Opin Biomed Eng* 7:1–8.
23. Gilleron J, et al. (2013) Image-based analysis of lipid nanoparticle-mediated siRNA delivery, intracellular trafficking and endosomal escape. *Nat Biotechnol* 31:638–646.
24. Wittrup A, et al. (2015) Visualizing lipid-formulated siRNA release from endosomes and target gene knockdown. *Nat Biotechnol* 33:870–876.
25. Akinc A, Battaglia G (2013) Exploiting endocytosis for nanomedicines. *Cold Spring Harb Perspect Biol* 5:a016980.
26. Chen D, et al. (2012) Rapid discovery of potent siRNA-containing lipid nanoparticles enabled by controlled microfluidic formulation. *J Am Chem Soc* 134:6948–6951.
27. Madisen L, et al. (2010) A robust and high-throughput Cre reporting and characterization system for the whole mouse brain. *Nat Neurosci* 13:133–140.
28. Zetsche B, et al. (2015) Cpf1 is a single RNA-guided endonuclease of a class 2 CRISPR-Cas system. *Cell* 163:759–771.
29. Doudna JA, Charpentier E (2014) Genome editing. The new frontier of genome engineering with CRISPR-Cas9. *Science* 346:1258096.
30. Hsu PD, Lander ES, Zhang F (2014) Development and applications of CRISPR-Cas9 for genome engineering. *Cell* 157:1262–1278.
31. Sahay G, et al. (2013) Efficiency of siRNA delivery by lipid nanoparticles is limited by endocytic recycling. *Nat Biotechnol* 31:653–658.
32. Dahlman JE, et al. (2014) In vivo endothelial siRNA delivery using polymeric nanoparticles with low molecular weight. *Nat Nanotechnol* 9:648–655.
33. Ronan T, Qi Z, Naegle KM (2016) Avoiding common pitfalls when clustering biological data. *Sci Signal* 9:re6.

34. Mui BL, et al. (2013) Influence of polyethylene glycol lipid desorption rates on pharmacokinetics and pharmacodynamics of siRNA lipid nanoparticles. *Mol Ther Nucleic Acids* 2:e139.
35. Geijtenbeek TB, et al. (2000) DC-SIGN-ICAM-2 interaction mediates dendritic cell trafficking. *Nat Immunol* 1:353–357.
36. Huang MT, et al. (2006) ICAM-2 mediates neutrophil transmigration in vivo: Evidence for stimulus specificity and a role in PECAM-1-independent transmigration. *Blood* 107:4721–4727.
37. Sager HB, et al. (2016) RNAi targeting multiple cell adhesion molecules reduces immune cell recruitment and vascular inflammation after myocardial infarction. *Science Transl Med* 8:342ra380.
38. Hendel A, et al. (2015) Chemically modified guide RNAs enhance CRISPR-Cas genome editing in human primary cells. *Nat Biotechnol* 33:985–989.
39. Platt RJ, et al. (2014) CRISPR-Cas9 knockin mice for genome editing and cancer modeling. *Cell* 159:440–455.
40. Brinkman EK, Chen T, Amendola M, van Steensel B (2014) Easy quantitative assessment of genome editing by sequence trace decomposition. *Nucleic Acids Res* 42:e168.
41. Palm W, Thompson CB (2017) Nutrient acquisition strategies of mammalian cells. *Nature* 546:234–242.
42. Kauffman KJ, et al. (2018) Rapid, single-cell analysis and discovery of vectored mRNA transfection in vivo with a loxP-flanked tdTomato reporter mouse. *Mol Ther Nucleic Acids* 10:55–63.
43. Kheirolomoom A, et al. (2015) Multifunctional nanoparticles facilitate molecular targeting and miRNA delivery to inhibit atherosclerosis in ApoE(-/-) mice. *ACS Nano* 9: 8885–8897.
44. Greineder CF, et al. (2018) Site-specific modification of single-chain antibody fragments for bioconjugation and vascular immunotargeting. *Bioconjug Chem* 29:56–66.
45. Sager HB, et al. (2016) Proliferation and recruitment contribute to myocardial macrophage expansion in chronic heart failure. *Circ Res* 119:853–864.